RESEARCH ARTICLE

Inkjet-Printed Lenses with Adjustable Contact Angle to Improve the Light Out-Coupling of Organic Light-Emitting Diodes

Ian Sachs, Marc Fuhrmann, Inge Verboven, Indranil Basak, Wim Deferme, and Hildegard Möbius*

The enhancement of the out-coupling efficiency of organic light-emitting diodes (OLEDs) is still the subject of research and development. Bottom-emission OLEDs emit light through the glass substrate into air. Due to the difference of the refractive indices between glass and air, a significant amount of light is reflected at the glass–air interface back into the glass because of total internal reflection. One possibility to avoid total internal reflection at the glass–air interface is the use of lenses. Herein, the concept of macrolenses for pixelated OLEDs is presented. For the design of the lenses, the vertical and horizontal dimensions of the OLED have to be considered, and the contact angle of the lens has to be adapted to the geometrical conditions. A process based on inkjet etching and inkjet printing has been developed which now allows the printing of lenses with defined radius and contact angle. Measurements of the luminance show an improved out-coupling efficiency.

I. Sachs, M. Fuhrmann, Prof. H. Möbius
Department of Computer Science/Micro Systems Technology
University of Applied Sciences Kaiserslautern
Amerikastraße 1, 66482 Zweibrücken, Germany
E-mail: hildegard.moebius@hs-kl.de

I. Verboven, I. Basak, Prof. W. Deferme
Functional Materials Engineering (FME)
Hasselt University
Wetenschapspark 1, B-3590 Diepenbeek, Belgium

I. Verboven, I. Basak, Prof. W. Deferme
Institute for Materials Research (IMO)
Wetenschapspark 1, B-3590 Diepenbeek, Belgium

I. Verboven, I. Basak, Prof. W. Deferme
Department of the Interuniversity MicroElectronics Centre, Leuven (IMEC)
The Institute for Materials Research in MicroElectronics (IMOMEC)
Wetenschapspark 1, B-3590 Diepenbeek, Belgium

The ORCID identification number(s) for the author(s) of this article can be found under https://doi.org/10.1002/adem.202100212.

1. Introduction

In recent years, significant improvements have been made toward organic light-emitting diodes (OLEDs) for the next generation of planar light sources.[1–4] Promising results are obtained by bottom-emission OLEDs that emit light through the substrate glass into air,[5] but the out-coupling of photons through this stack of layers including the glass substrate is limited. Therefore, the enhancement of out-coupling efficiency has been subject of intensive research and various methods have been proposed.[1] One focus is on the improvement of the out-coupling efficiency at the glass–air interface. The large differences among the refractive indices of glass and air result in total internal reflection at the substrate–air interface. A significant amount of light is trapped in the substrate, which reduces the devices efficiency and light output.[6] Assuming a refractive index of glass with $n = 1.5$ OLEDs with a conventional planar structure limits the light extraction efficiency due to total internal reflection of the glass–air interface to about 53.4%.[7] Various substrate modification techniques have been suggested to reduce these wave-guiding effects. The simplest modification to improve the out-coupling is the usage of rough surfaces,[8–10] which can increase the external quantum efficiency by a factor up to four.[11] Intensive research activities are focused on enhancing the out-coupling efficiency by structuring the surface, e.g., by cone structures[11] or spherically shaped structures on the back side of the glass substrate increasing the factor of the out-coupling from 1.5 to 3.0.[2,5,9,12,13] Hemispherically shaped structures smaller than the OLED diameter are defined as microlenses. There are various efforts to optimize microlenses and microlens arrays by variation of the lens structure, shape of the lenses,[2] contact angle (CA),[14,15] and gap between the microlenses.[12] Kim et al.[15] showed an improvement of luminance by a factor of 2 by using lenses of a different shape and CA. On the contrary, lenses with dimensions equal or larger than the OLED are defined as macrolenses, acting as an index-matching material to avoid total internal reflection as well as lenses focusing the radiation.[1,6,9] However, by using macrolenses, only rays coming from the centre of the OLED impinge normally on the substrate–air interface but for rays coming from areas close to the edge of

**ADVANCED
SCIENCE NEWS**

www.advancedsciencenews.com

**ADVANCED
ENGINEERING
MATERIALS**

www.aem-journal.com

the OLED total internal reflection will still occur. Therefore, one solution to improve the out-coupling of light at the glass–air interface is the use of pixelated OLEDs, which are smaller than the lens structure.[2,6] State-of-the-art processes to fabricate micro/macrolenses (or arrays) can be subdivided into three typical classes: 1) surface-tension-driven approaches using melt-reflow or inkjet printing, 2) imprinting approaches, and 3) lithography processes.[16] The best-known processes are photolithography processes using grayscale or interference grayscale lithography.[17–20] To reduce the complexity, the lens array can be created by using focussed ion beam or hot embossing processes to directly fabricate the pattern onto the substrate material.[21] Another approach is the usage of stamps or mould transfer processes.[22,23] However, these processes are either not suitable for mass production, expensive, or not easily adaptable. That means the material waste is high and design changes are difficult to fulfill. Therefore, drop on demand (DoD) inkjet printing suits this application, as the lens can be printed directly on the substrate and fine tuning of the lenses is easily feasible according to Lin et al.[24] by tuning the lens parameters using an inkjet printing process to adjust the position of the lens freely and using different materials.

The aim of this work is to discuss the concept of macrolenses for pixelated OLEDs and to demonstrate the fabrication of optimized macrolenses by adjusting the CA of the lenses. The lenses are fabricated in a two-step process using inkjet etching and printing developed by Cramer et al.[25] First, a ring-shaped reservoir is created using the coffee-ring effect followed by inkjet printing of the lens material. In this work, the process developed by Cramer et al.[25] is expanded by the introduction of two surface enhancement steps. Using suitable substrate enhancement processes, such as silanization, the CA can be adapted in the range from 30° to 90°. Thus, the CA can now be optimized and adjusted to the size parameters of the pixelated OLED and was proven to lead to an enhanced out-coupling efficiency.

2. Experimental Section

The OLED stack used consists of the layers and materials to be found in **Table 1**.

To characterize the printing process, a profilometer (DektakXT from Bruker Cooperation) was used. To get a 3D image of the topography, a map scan was made (Table S1, Supporting Information).

A printing process for the lenses, respectively, an etching process for the creation of the reservoirs was established using the inkjet printer Dimatix DMP-2831, FujiFilm Dimatix Inc. to create reproducible lenses and reservoirs for the lens containment. To enhance the substrate's properties for the printing process, two types of silane were used as follows: APTES (3-aminopropyl)triethoxysilane 99%, Sigma-Aldrich, and FOTCS trichloro(1H,1H,2H,2H-perfluorooctyl)silane 97%, Sigma-Aldrich. The ink (cf., **Table 2**) used for the etching process consisted of $CH_3OC_6H_5$ (anisole, anhydrous, 99.7% Sigma-Aldrich) and the ink for the lens material consisted of NOA89 (Norland Optical Adhesive 89, Norland Products Inc.). Finding and tuning the parameters, as shown in **Table 3**, was the critical step for the development of the process.

3. Theory

The typical OLED consists of a layer stack of a planar glass substrate frequently covered by ITO (indium tin oxide) as an anode, a hole injection and transport layer (HIL/HTL), an organic emitter (EML), an electron injection and transport layer (EIL/ETL), and the cathode. The materials used in the stack possess different refractive indices n for each layer[26] (Table 1, **Figure 1**). Therefore, total internal reflection occurring at the interfaces of layers with different refractive indices leads to reduced light out-coupling of the OLED. For angles larger than the critical angle of total internal reflection, the rays are completely reflected. This article focusses on the glass–air interface and the possibility to avoid total internal reflection for pixelated OLEDs at this interface to enhance the light out-coupling (Figure 1). As discussed in the introductory part of this article, one possibility to reduce the loss through total internal reflection at the glass–air interface are macrolenses. Macrolenses are defined as lenses with dimensions equal or larger than the lateral size of the OLED as shown in Figure 1.

Table 1. Materials in OLED Stack.[29–31]

Layer	Type	Thickness	Refractive index
Lens material	Optical adhesive NOA89, Norland, Inc.	Inkjet printed, ≈1–2 mm (highest point, depending on CA)	1.5
Lens substrate (support)	Plexiglas Film Clear 99524 GT, Röhm AG	Height: up to 40 μm, substrate: foil, thickness: 250 μm	1.49
Glass substrate with anode	Floating glass with In_2O_3–SnO_2 (ITO)	Glass: 1 mm ±0.1 ITO, pvd: 250 nm ± 25	Glass: 1.52 ITO: 1.83
Hole transport layer	Poly(3,4-ethylenedioxythiophene)-poly(styrenesulfonate) (PEDOT:PSS) Sigma-Aldrich	Spin coated, 30 nm	1.52
Emitting layer	Phenyl-substituted poly(para-phenylenevinylene) copolymer (Super yellow (SY)), Sigma-Aldrich	Spin coated, 80 nm	2.1
Electron injection/transport	Ca		
Cathode (metallic)	Al	250 nm in total, pvd	-

Table 2. Ink parameters.

	Dimatix requirement	Anisole	NOA89
Viscosity	10 cps–12 cps	1.52 cps @ 15 °C 0.778 cps @ 30 °C	15 cps–20 cps @ 25 °C
Surface tension	28–30 dyne cm^{-1}	36.18 dynecm^{-1} @ 15 °C 34.15 dynecm^{-1} @ 30 °C	n/a
Particle size	<1 μm	None	None
pH	≈7	7	7
Temperature	Up to 60 °C	Boiling point = 154 °C	−60–125 °C

Table 3. Printing parameters.

	Reservoir	Lens
Nozzles	Up to 4	Up to 4
Firing voltage	14.13 V ± 0.26	13.14 V ± 0.64
Cartridge height	320 μm	500–1500 μm
Substrate thickness	250 μm	250–1000 μm
Substrate temperature	RT	Up to 35 °C
Drop spacing	10 μm	10 μm
Layers	20	15–30 @ $d_{printarea}$ = 3.1–4 mm
Cartridge temperature	20–28 °C	45 °C
Room temperature	21 ± 4 °C	21 ± 4°
Drop volume	10 pL	10 pL
Meniscus point	3.5	5.0
Cleaning cycle	Before print	Before print
Surface enhancement	APTES (3-aminopropyl) triethoxysilane	FOTCS trichloro(1 H,1 H,2 H-perfluorooctyl)silane

Light emitted from the EML will leave the OLED at angles less than the critical angle of total internal reflection θ_c given by

$$\theta_c = \sin^{-1}\left(\frac{n_{air}}{n_{glass}}\right) \tag{1}$$

Assuming the refractive index of glass $n_{glass} = 1.5$ and of air $n_{air} = 1.0$, the critical angle of total internal reflection θ_c equals to 41.8°. Light emitted at angles larger than this critical angle will be trapped in the substrate (Figure 1).

Using lenses in the shape of a hemisphere with an emitting point like light source at its centre, all rays are impinged normally to the lens–air interface thus avoiding total internal reflection completely. However, OLEDs are lateral extended light sources (cf., Figure 1, d_{light}) and consist of a layer stack as described earlier leading to an increased horizontal and vertical distance between emitting light source and the centre of the lens (cf., Figure 1 and **2**).

Thus, as shown in Figure 2A, using a hemispherical lens with CA of 90° rays from the edge of the OLED will still be trapped in the OLED-lens system leading to a reduction of the light out-coupling. Reducing the CA of the lens, total internal reflection can be avoided for all rays from the extended OLED resulting in an enhanced out-coupling efficiency. The CA of the lens for an optimized design depends on the parameters of the OLED (lateral and vertical dimensions, materials) and the lenses (material, radius of the lens, and thickness of support layer) and has to be calculated and adjusted for each individual design. The calculations are based on the law of diffraction and the phenomenon of total internal reflection.

4. Results and Discussion

The fabrication of the lenses consists of five steps: enhancing the substrate, creation of the reservoir, intermediation enhancement of the inter-reservoir substrate, inkjet printing, and lens curing. The following flowchart shows the process flow.

To fabricate macrolenses with defined CAs, the three-step process developed by Cramer et al.[25] is used and supplemented
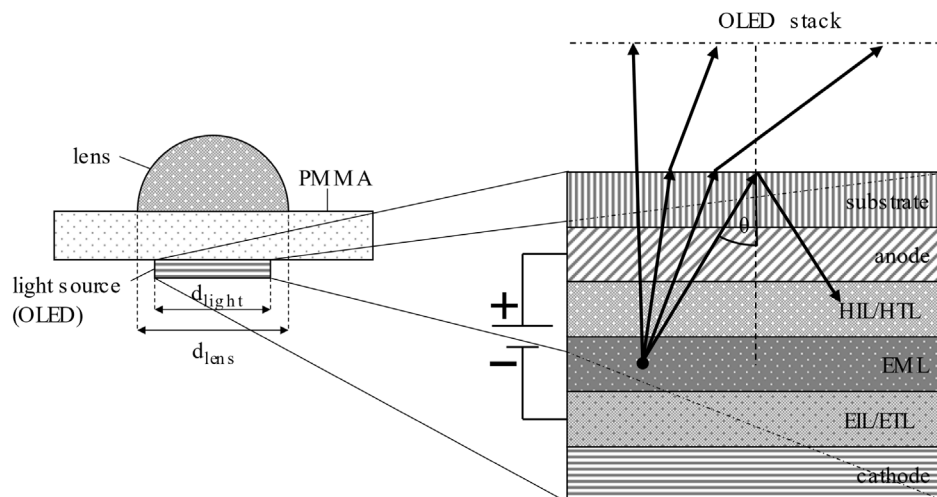

Figure 1. Macrolens ($d_{lens} \geq d_{light}$) with OLED stack (right side zoomed; HIL/HTL: hole injection/transport layer; EML: emissive layer; EIL/ETL: electron injection/transport layer). Arrows demonstrate the rays emitted in the OLED and the total internal reflection occurring at the glass–air interface.
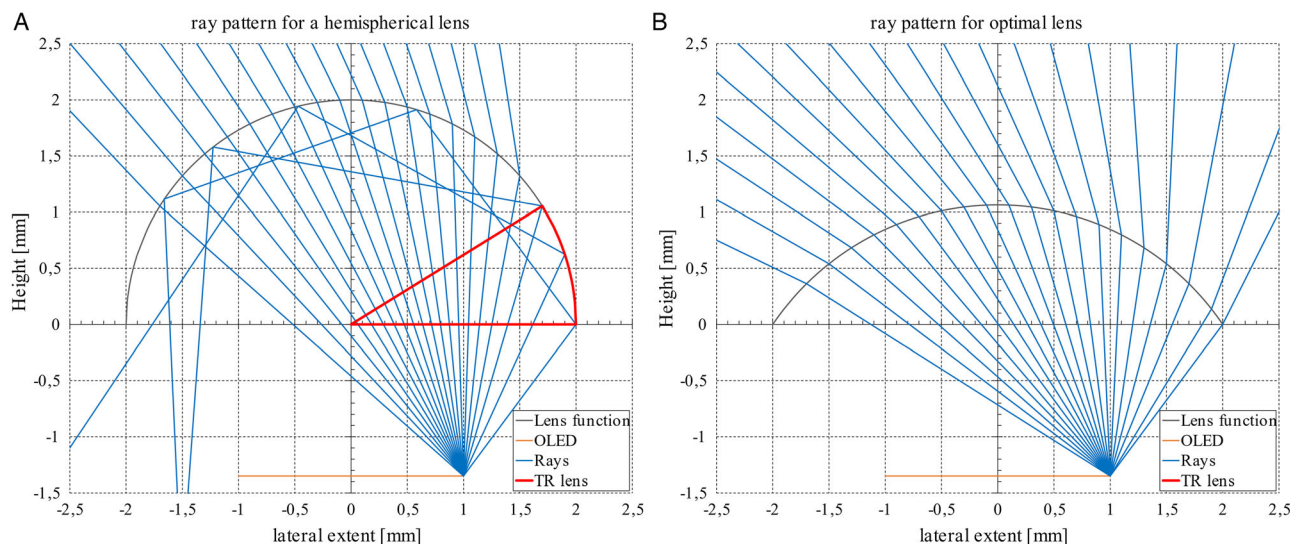
Figure 2. A) Hemispherical lens (CA 90°) with total internal reflection (TR); B) the red triangle shows the area of rays lost because of total internal reflection right: calculated optimal lens with a CA of 56°; all rays leave the lens at the lens–air interface.
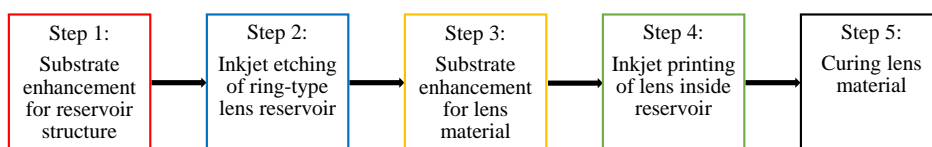
Figure 3. Overview of the fabrication process for the inkjet-printed lenses.
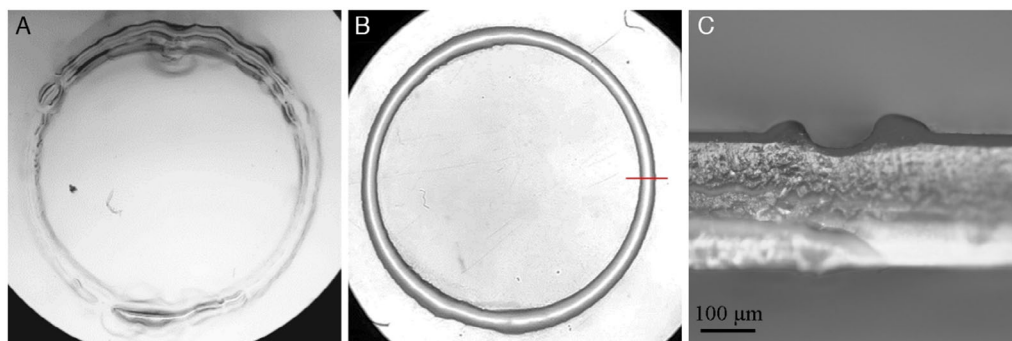
Figure 4. A) Untreated PMMA substrate after inkjet etching using anisole; B) substrate treated with silane APTES; right: cross section of inkjet-etched reservoir wall structure (red section) (microscope, ring diameter $d_{ring} = 4\ mm$); C) cross section of the ring structure (vertical cut, microscope).

by introducing two surface enhancement steps using the silanization process (step 1 and step 3 in **Figure 3**).

4.1. Substrate Enhancement for Reservoir Structure

As substrate for the lens, a 250 µm thick polymethyl methacrylate (PMMA) foil is used (Table 1).

In the first step, the PMMA surface has to be prepared for the second step, the inkjet etching of ring-shaped reservoir structure. As anisole is used to inkjet etch PMMA, the wetting behavior of anisole on PMMA is of importance. Using non-surface-enhanced

PMMA anisole leads to wetting of the ink on the surface and a blurred printing pattern (**Figure 4** left) in the second process step. By modifying the surface using APTES ((3-aminopropyl) triethoxysilane) (see "the Experimental Section"), the line sharpness can be increased and it is now possible to create homogeneous wall structures as shown in Figure 4.

4.2. Inkjet Etching of Ring-Type Lens Reservoir

The lens reservoir is created by inkjet etching. The substrate used is the surface-enhanced PMMA foil of step 1, which can be

**ADVANCED
SCIENCE NEWS**

www.advancedsciencenews.com

**ADVANCED
ENGINEERING
MATERIALS**

www.aem-journal.com

etched with anisole[24] using the printing parameters in Table 3. The principle of inkjet etching is shown in **Figure 5**: the dissolved PMMA will be transported to the edge of an anisole droplet induced by faster evaporation rates at the edge of the droplet. The dried PMMA creates a wall in form of a ring. This is well known as the coffee stain effect.[27,28]

The process of inkjet etching increases the roughness of the PMMA from $rms = 0.0141\,\mu m$ for the untreated PMMA to $rms = 1.983\,\mu m$ within the etched structure as shown in **Figure 6**.

Therefore, instead of printing a big droplet for the creation of the lens reservoir, it is necessary to inkjet etch a ring (**Figure 7**) to avoid the increase in the surface roughness within the reservoir. The ring-shaped printing pattern preserves the low roughness of

the substrate on the inside of the reservoir, where the lens will be placed and thus unwanted light scattering at the PMMA–lens interface can be avoided.

Inkjet etching a ring to preserve the low roughness of the PMMA inside the reservoir leads to a ring-shaped double wall structure as shown in Figure 7.
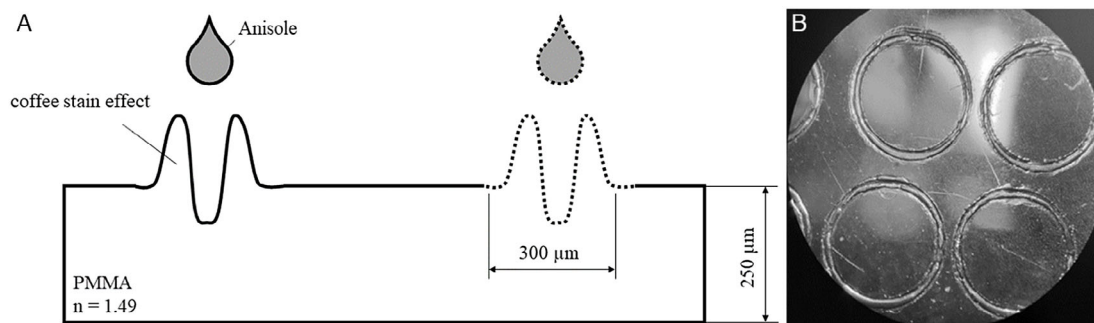
The structural height of the reservoir is in the range of tens of microns. The more anisole is used for etching, the stronger the coffee ring effect and thus the higher the wall. Therefore, several printing steps of anisole are necessary. As the number of layers printed on the substrate is directly connected to the amount of material printed, the reservoir height can be tuned. Furthermore, the line thickness of the printed pattern, the
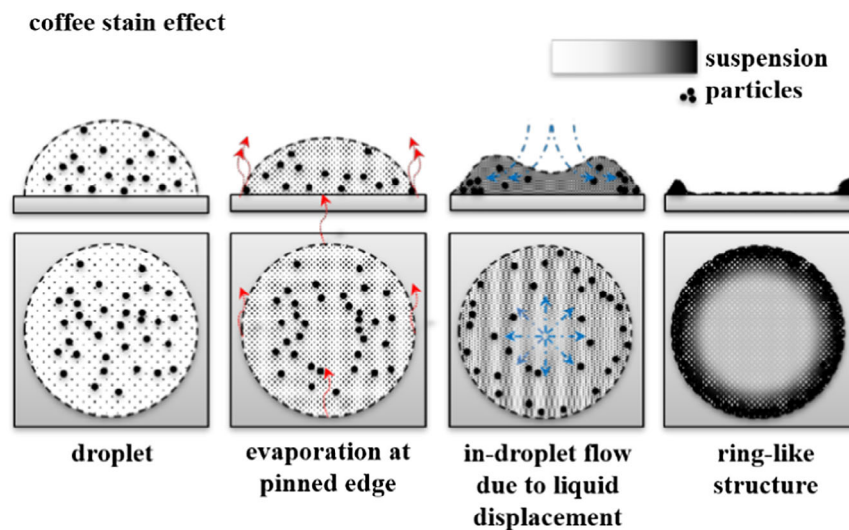

Figure 5. Coffee stain effect—transporting material toward the edges of the droplet.
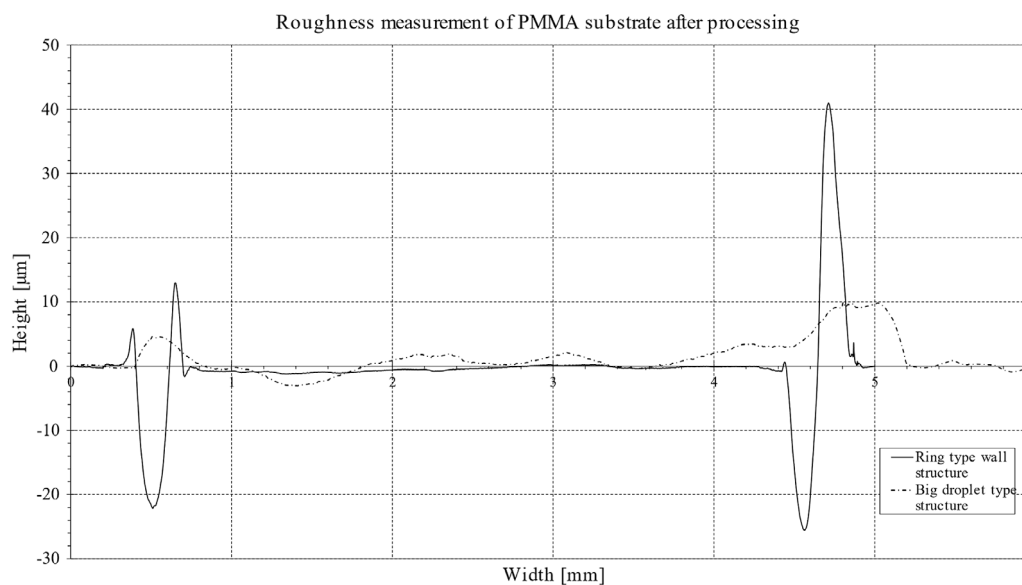
Figure 6. Topography measurement of inkjet-etched PMMA—solid: ring-type structure; dashed: big droplet of anisole (DektakXT).

2100212 (5 of 9)

**ADVANCED
SCIENCE NEWS**
www.advancedsciencenews.com

**ADVANCED
ENGINEERING
MATERIALS**
www.aem-journal.com

Figure 7. A) Schematic figure of inkjet-etched reservoir structure with double-sided walls; B) top view of etched reservoir structure on PMMA (microscope, $d_{ring} = 4$ mm). Reproduced with permission[25] Copyright 2018, SPIE Photonics Europe.
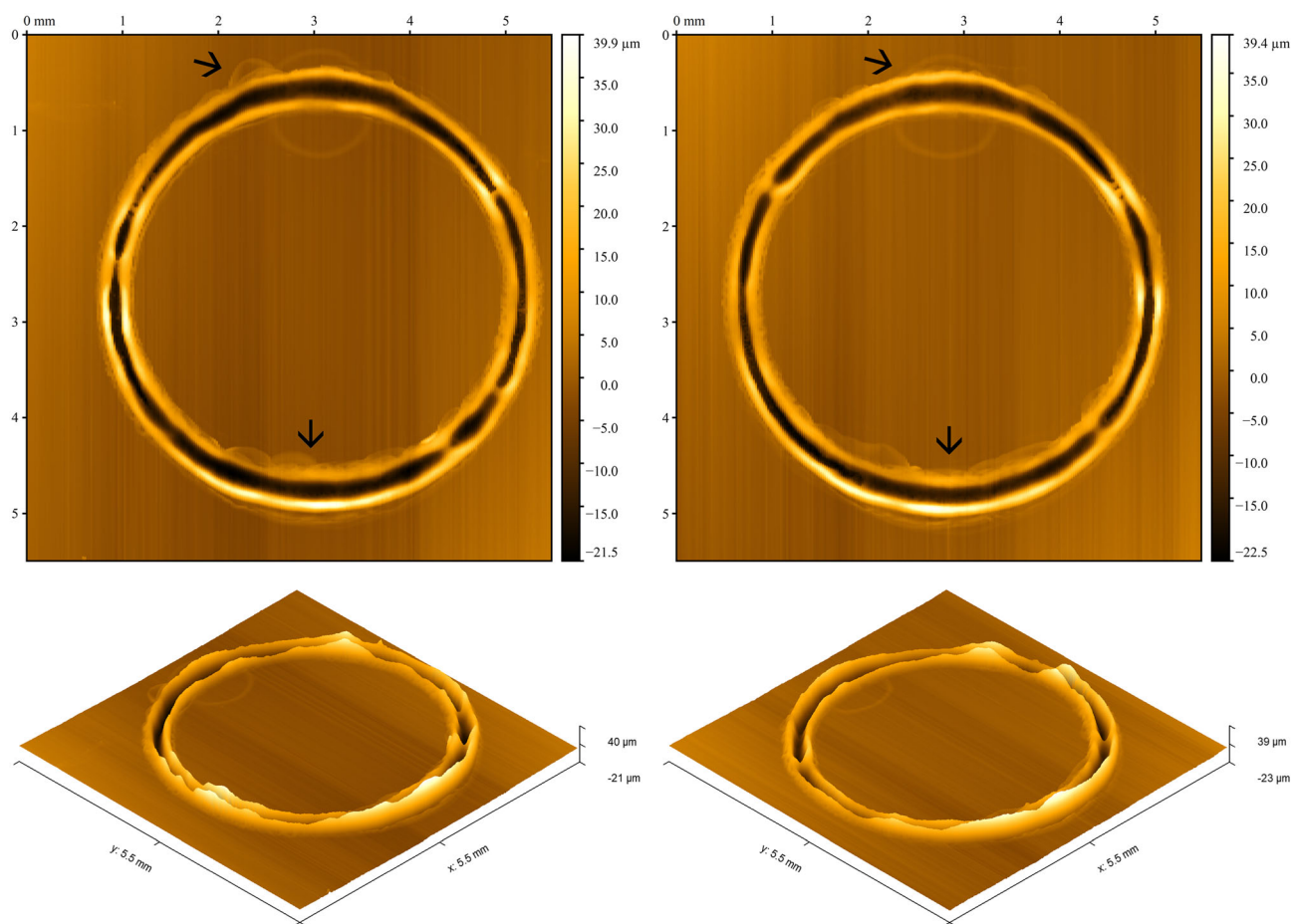
Figure 8. View of the reservoir (top and side) using DektakXT profilometer, arrows showing defects.

temperature adjustments, the number of nozzles used, and the piezo voltage show a small dependency on the structural height. **Figure 8** shows the measured topography of the reservoir structure.

Some positions (see arrows in Figure 8) show a blurred printing pattern at the same position throughout all samples. As line wise is printed (Cartesian system: x printed first, then y moved according to resolution setting), the material amount (at a given time interval) at these points is higher than at the other points. These irregularities showed no influence for the use of the structure as a lens reservoir.

4.3. Substrate Enhancement for Lens Material

In addition, the printing process of the lens material NOA89 (Table 1–3) needs be enhanced by silanization to increase the lens'

ADVANCED
SCIENCE NEWS
www.advancedsciencenews.com

ADVANCED
ENGINEERING
MATERIALS
www.aem-journal.com

Figure 9. A) Untreated PMMA substrate with droplet of NOA89 (lens material) wetting the surface; B) substrate modified with silane APTES; C): using FOTCS as silane (see Table 3).

CA (**Figure 9**A-C), as the CA is limited by the wetting of the lens material. For this process step, FOTCS (trichloro(1 H,1 H,2 H, 2 H-perfluorooctyl)silane) is used for silanization.

Printing NOA89 on untreated PMMA substrates leads to complete wetting of the ink on the surface (Figure 9A) as NOA89 is an adhesive, therefore good wetting properties are needed. Silanization using APTES, the silane applied in the first silanization step for the reservoir etching increases the CA to $CA_{APTES} = 13.9°$ (Figure 9B), which still is too low for desired lenses (cf. Figure 11). As shown in Figure 9C, the use of FOTCS for silanization increases the CA to $CA_{FOTCS} = 44.3° \pm 0.9$, which is necessary for the lens deposition in the next step.

4.4. Inkjet Printing of Lens Inside Reservoir

The second printing step creates the lens itself (**Figure 10**). The lens material (NOA89) is inkjet printed inside the reservoir creating a lens with defined diameter and adjustable CA. It is directly depending on the amount of material and therefore on the number of printed layers. By changing the amount of printed material, the CA can be increased even above 90°.

NOA89 is an optical adhesive with high transparency for visible light (>99%) and sufficient physical properties for inkjet printing (see Table 2 and 3). The ring-shaped reservoir structure printed in the first step was used as a container for the lens material.

The most critical step in printing the lenses is the alignment and the size of the pattern inside the reservoir. Lenses with high
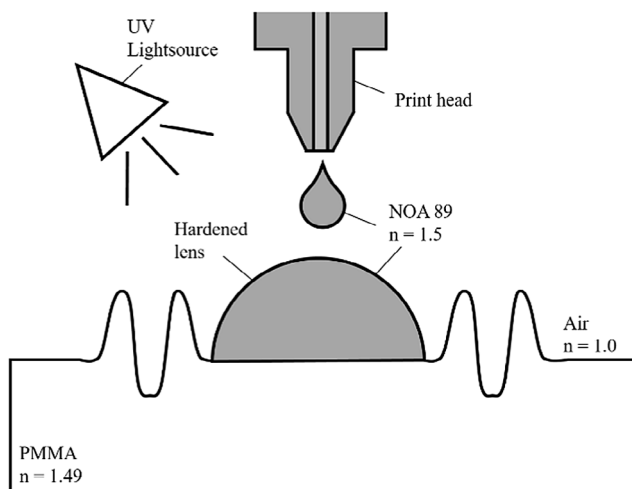
CA and therefore more material have more liquid mass and tend to spread more easily by gravity. Therefore, to avoid spreading above the reservoir wall and in contrast to guarantee a homogeneous spreading on the PMMA, the diameter of the printing pattern must be adjusted to the desired CA of the lens (see the Supporting Information).

Figure 11 shows the necessity of process step 4 for creating high CAs and compares the effect of the two silanes APTES and FOTCS used for surface enhancement (Table 3).

Silanization with FOTCS allows to fabricate lenses with CAs larger than 90° whereas silanization with APTES only achieves CAs in the range of 30° as with APTES it is not possible to print more than six layers without the lens material to yield out of the reservoir.
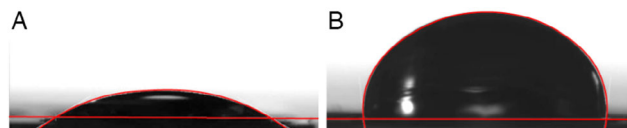
Figure 12 shows the CA of the lens as a function of the number of printed layers where nearly linear behavior is observed.
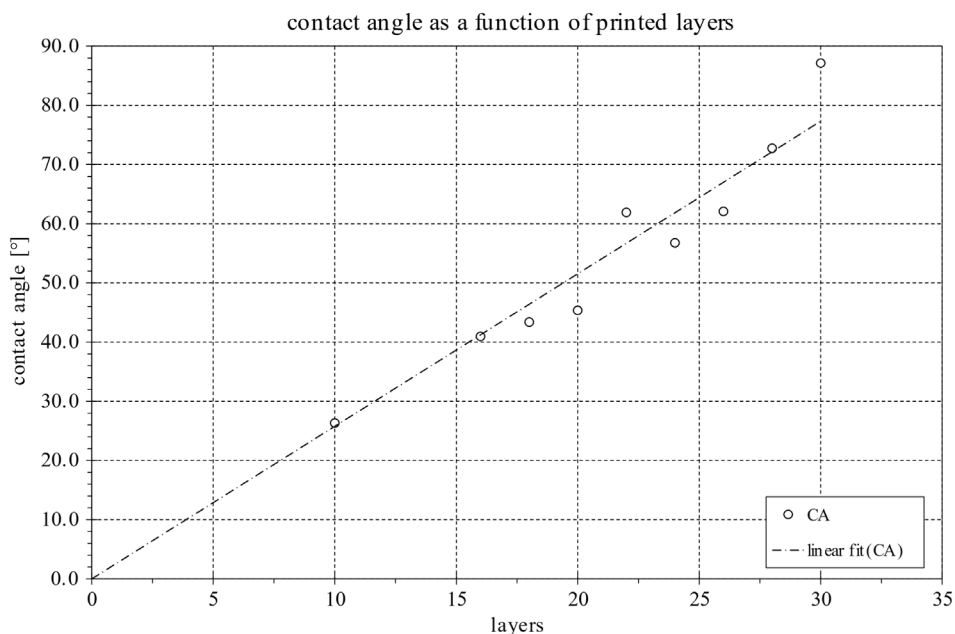
4.5. Curing Lens Material

After the printing process, the material needs to be cured with UV light (wavelength $\lambda = 366$ nm) (step five in Figure 3). To reduce the heat output of the UV light source and prevent heat-induced cracking of NOA89, an LED with $\lambda_{PEAK} = 395-405$ nm was used (Helixeon 3535 LED). The output of the LED was 3.45 V and 400 mA. The curing time was adapted to the CA of the lens with a maximum curing time of ≈ 1 h. The curing process showed no changes in the CA measurement, demonstrating that no volume loss occurred.

Thus, using the five-step fabrication process, the parameters of the lens now can be tuned: the lens radius is defined by the size of the reservoir and the CA is given by the number of printed layers.
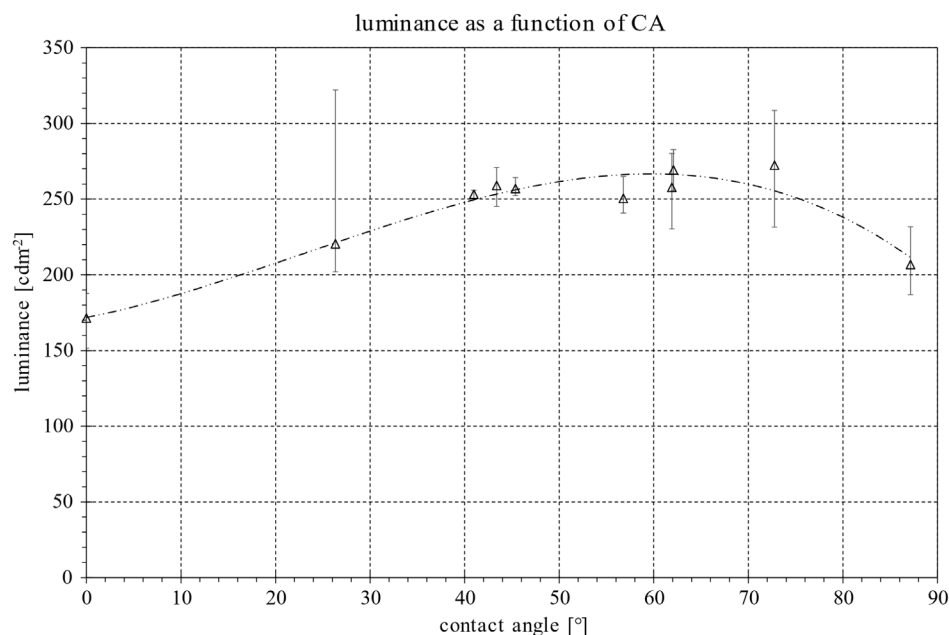
Figure 13 shows the luminance of the OLEDs as function of the CA of the lens. Without using a lens (CA equals zero), the luminance equals $L_V = 171.4$ cd m^{-2} (at approximately $U = 8$ V, $I = 52$–75 mA). By applying a lens to the substrate with $CA_{lens} = 30°$, the luminance increases by 47.7%. A further increase in the CA leads to a maximum of luminance observed between a CA of 60° and CA of 70°. A further increase in the CA toward 90° leads to a decrease in luminance. This behavior,

Figure 10. Schematic view of inkjet printing of the macrolens and curing inside the reservoir. Reproduced with permission[25] Copyright 2018, SPIE Photonics Europe.

Figure 11. A) APTES-enhanced PMMA substrate with lens in reservoir structure ($CA_{R\_FOTCS} = 32.25° \pm 0.05$); B) FOTCS ($CA_{R\_FOTCS} = 95.9° \pm 1.2$).

**ADVANCED
SCIENCE NEWS**

www.advancedsciencenews.com

**ADVANCED
ENGINEERING
MATERIALS**

www.aem-journal.com

Figure 12. Printed layers as a function of the CA.

Figure 13. Luminance as a function of the CA.

indicated in a trend line in Figure 13, is in accordance with theory expecting a maximal out-coupling efficiency for CAs less than 90 degrees due to total internal reflection as discussed in Section 3.

In summary, introducing macrolenses with radius and CA adjusted to the vertical and horizontal dimensions of the pixelated OLED, it is possible to avoid the total internal reflection at the glass–air interface and thus to enhance the light out-coupling by a factor of ≈1.6.

5. Conclusion and Outlook

The aim of this work was to enhance the out-coupling efficiency of pixelated OLEDs by avoiding total internal reflection at the substrate–air interface with the help of lenses with optimized CAs adjusted to the size parameters of the OLED. Already existing inkjet etching and inkjet printing processes were optimized by introducing two substrate enhancement

2100212 (8 of 9)

steps which now allow the fabrication of macrolenses for pixelated OLEDs with tuneable size and CA. Inkjet etching based on the coffee ring effect was used to create reservoirs for the lenses. To avoid blurred printing patterns due to wetting effects, a first substrate enhancement step was introduced before inkjet etching the reservoir. Printing a ring instead of printing a big droplet helps to keep the low surface roughness inside the reservoir to prevent unwanted light scattering. A second surface enhancement process was introduced before printing the lens material. As the CA is limited by the wetting of the lens material on the PMMA, foil silanization is necessary to achieve high CAs. Using this process, the CA of the lenses can now be varied in the range from 30° to 90°. The optimization of the CA by adjustment to the size parameters of the OLED was proven to enhance the out-coupling efficiency by a factor of 1.6. As the lens' CA can easily be changed by the number of printed layers, this method now offers a flexible method to print lenses in general for various applications.

Conflict of Interest

The authors declare no conflict of interest.

Data Availability Statement

Research data are not shared.

[1] K. Saxena, V. K. Jain, D. S. Mehta, *Opt. Mater.* **2009**, *32*, 221.
[2] B. Riedel, I. Kaiser, J. Hauss, U. Lemmer, M. Gerken, *Opt. Express* **2010**, *18*, A631.
[3] T. Komoda, H. Sasabe, J. Kido, in *The Proc. of AM-FPD 18: The Twenty-fifth Int. Conf. on Active-Matrix Flatpanel Displays and Devices – TFT Technologies and FPD Materials*, IEEE, Piscataway, NJ **2018**, pp. 1–4.
[4] A. Salehi, X. Fu, D.-H. Shin, F. So, *Adv. Funct. Mater.* **2019**, *29*, 1808803.
[5] N. Danz, C. A. Wächter, D. Michaelis, P. Dannberg, M. Flämmich, *Opt. Express* **2012**, *20*, 12682.
[6] C. F. Madigan, M.-H. Lu, J. C. Sturm, *Appl. Phys. Lett.* **2000**, *76*, 1650.
[7] S. Lloyd, T. Tanigawa, H. Sakai, H. Murata, *IEICE Trans. Electron.* **2019**, *E102.C*, 180.
[8] N. K. Patel, S. Cina, J. H. Burroughes, *IEEE J. Select. Topics Quantum Electron.* **2002**, *8*, 346.
[9] D. S. Mehta, K. Saxena, *Proc. of ASID'06: Light out-coupling strategies in organic light emitting devices*, ASID'06, Asian Symp. on Information Display, New Delhi, India **2006**.
[10] S. Chen, H. S. Kwok, *Opt. Express* **2010**, *18*, 37.
[11] G. Gu, D. Z. Garbuzov, P. E. Burrows, S. Venkatesh, S. R. Forrest, M. E. Thompson, *Opt. Lett.* **1997**, *22*, 396.
[12] M.-K. Wei, I.-L. Su, *Opt. Express* **2004**, *12*, 5777.
[13] H. Peng, Y. L. Ho, X.-J. Yu, M. Wong, H.-S. Kwok, *J. Display Technol.* **2005**, *1*, 278.
[14] H. Ren, S.-T. Wu, *Opt. Express* **2008**, *16*, 2646.
[15] H. S. Kim, S. I. Moon, D. E. Hwang, K. W. Jeong, C. K. Kim, D.-G. Moon, C. Hong, *Opt. Laser Technol.* **2016**, *77*, 104.
[16] E. P. Chan, A. J. Crosby, *Adv. Mater.* **2006**, *18*, 3238.
[17] T. J. Suleski, D. C. O'Shea, *Appl. Opt.* **1995**, *34*, 7507.
[18] M.-H. Wu, C. Park, G. M. Whitesides, *Langmuir* **2002**, *18*, 9312.
[19] M. V. Kunnavakkam, F. M. Houlihan, M. Schlax, J. A. Liddle, P. Kolodner, O. Nalamasu, J. A. Rogers, *Appl. Phys. Lett.* **2003**, *82*, 1152.
[20] K. Zhong, Y. Gao, F. Li, Z. Zhang, N. Luo, *Optik* **2014**, *125*, 2413.
[21] N. Ong, Y. Koh, Y. Fu, *Microelectron. Eng.* **2002**, *60*, 365.
[22] S. Möller, S. R. Forrest, *J. Appl. Phys.* **2002**, *91*, 3324.
[23] C.-Y. Chang, S.-Y. Yang, M.-H. Chu, *Microelectron. Eng.* **2007**, *84*, 355.
[24] X. Lin, A. Hosseini, X. Dou, H. Subbaraman, R. T. Chen, *Opt. Express* **2013**, *21*, 60.
[25] W. Deferme, M. Cramer, J. Drijkoningen, I. Verboven, in *Organic Electronics and Photonics: Fundamentals and Devices* (Eds: S. Reineke, K. Vandewal), SPIE, Bellingham, WA **2018**, p. 34.
[26] B. Geffroy, P. Le Roy, C. Prat, *Polym. Int.* **2006**, *55*, 572.
[27] R. D. Deegan, O. Bakajin, T. F. Dupont, G. Huber, S. R. Nagel, T. A. Witten, *Nature* **1997**, *389*, 827.
[28] D. Tam, V. von Arnim, G. H. MCKINLEY, A. E. Hosoi, *J. Fluid Mech.* **2009**, *624*, 101.
[29] C. -S. Wu, C. -Y. Chou, Y. Chen, *J. Mater. Chem. C* **2014**, *2*, 6665.
[30] T. A. F. König, P. A. Ledin, J. Kerszulis, M. A. Mahmoud, M. A. El-Sayed, J. R. Reynolds, V. V. Tsukruk, *ACS Nano* **2014**, *8*, 6182.
[31] C.-W. Chen, S.-Y. Hsiao, C.-Y. Chen, H.-W. Kang, Z.-Y. Huang, H.-W. Lin, *J. Mater. Chem. A* **2015**, *3*, 9152.